Turk J Chem
35 (2011) , 181 – 188.

doi:10.3906/kim-0911-325

Controlled growth of two-dimensional copper nanoplates in graphite gallery

Xiaobei BIN[1,2], Jiazang CHEN[3], Hong CAO[3,*]
[1] *College of Resources & Environment Engineering, Wuhan University of Technology, Wuhan, 430070, P.R.-CHINA*
e-mail: bxp2000@whut.edu.cn
[2] *Hubei Provincial Key Laboratory of Minerals Resources Processing and Environment, Wuhan, 430070, P.R. -CHINA*
[3] *School of Materials Science & Engineering, Wuhan Institute of Technology, Wuhan, 430074, P.R.-CHINA*
e-mail: caohong@mail.wit.edu.cn

Received 28.11.2009

Copper nanoplates embedded in a graphite gallery were obtained by in situ reduction of stage 1, stage 2, and stage 3 $CuCl_2$-graphite intercalation compound precursors. The characterization results indicated that the morphology of the copper species was that of a 2-dimensional or quasi-2-dimensional nanoplate in the graphite gallery. Interaction between the metallic nanoplates and graphene sheet was also detected. The hexagonal graphene network restricted the crystallization orientation of the copper nanoparticles, and, at the same time, the finite space between the graphene sheets prevented the increase of the thickness. This method would provide a convenient route to synthesize or assemble 2-dimensional metal nanoplates.

Key Words: Carbon-encapsulated, nanostructures, electron microscopy, Raman spectroscopy, X-ray diffraction

Introduction

The weak stacking between the layers of hexagonal graphene networks provides conditions for the growth of other species in the gallery. When the graphite is modified with low-dimensional metallic nanoscale species in the gallery, some excellent characteristics of graphite remain. Additionally, the modified graphite would

*Corresponding author

be able to provide several neonatal characteristics because of the interaction between the inserted metallic nanoparticles and the graphene network in the special gallery, i.e. the charge transfer from the embedded metallic nanoparticles to the host network. The combination of the intrinsic properties of graphite and the neonatal characteristics possesses some potential applications in several fields, such as selective catalysis,[1–4] hydrogen storage,[5] superconductivity,[6] 2-dimensional magnetism, and lubrication.[7–8] For example, when a graphene-encapsulated copper nanoparticle composite is employed as a solid-state lubricant, not only should the friction coefficient be lowered, but the wearing on the surface can also be repaired by metallic nanospecies.

So far, various graphene-encapsulated nanoparticles have been obtained by reduction of graphite intercalation compound (GIC) precursors with hydrogen,[9–13] metallic potassium,[14–15] KBH_4 solution,[16] and an organic solution of alkali metals.[17] In the present work, the graphene-encapsulated copper nanoplates were prepared by reduction of $CuCl_2$ graphite intercalation compounds in warm conditions. The interaction between the copper nanoplates and graphene, and the effects of graphene on controlling growth of the copper nanoplates in the gallery, are discussed.

Experimental

The starting material, $CuCl_2$-GIC, was obtained by the molten salt method according to a recent publication.[18] $CuCl_2$ was mixed with exfoliated graphite by ball milling, followed by heating at a desired temperature according to the target stage-structure of the GIC products. The detailed experimental parameters and sample numbers are listed in the Table. The obtained GICs were washed with ammonia and distilled water to remove the excessive CuCl and $CuCl_2$. The GIC precursor was then fluxed in an ethylenediamine solution containing KBH_4 reducing reagent at 60 °C for 2 h. After reaction, the solid product was washed with ethanol and distilled water repeatedly. Finally, the sample was washed with HCl-acidified $FeCl_3$ solution to remove the possible unencapsulated copper species. The sample was then filtered out and dried at 60 °C in a vacuum for further characterization.

Table. Experimental parameters and the chemical composition of samples.

Sample No.	Precursor	Chemical composition[a]					Size of copper (nm)		
		Element	C	Cu	Cl	K	Min.	Max.	Average
1	Stage 1 GIC Formed at 300 °C	Content (wt %)	68.71	18.85	4.30	8.13	7.2	51.8	22.5
		SD[b]	7.29	1.83	2.15	1.82			
2	Stage 2 GIC Formed at 320 °C	Content (wt %)	72.02	12.87	4.43	10.68	15.8	58.3	28.3
		SD	1.37	1.05	0.26	0.66			
3	Stage 3 GIC Formed at 450 °C	Content (wt %)	72.80	11.39	4.17	11.64	18.9	37.9	28.5
		SD	1.75	0.49	0.25	1.23			

[a] The product compositions were characterized using EDX; the concentration of boron in the samples was only a trance amount and was omitted here. [b] SD: standard deviation.

The as-prepared samples were characterized by X-ray diffraction (XRD) using CuKα radiation. Morphologies and compositions were characterized using a FEI Sirion 200 field emission scanning electron microscope

equipped with an energy dispersion spectrograph (EDAX Falcon). High-resolution transmission electron microscopy (HRTEM) characterization was carried out with a JEOL JEM-2100 field emission electron microscope at 200 kV accelerating voltage. XPS spectra were recorded with an ESCALAB MK II spectroscope. Raman spectroscopy was employed to investigate the variation of the hexagonal network of the graphite.

Results and discussion

Phase and chemical composition

Figure 1 shows the XRD pattern of sample 1 reduced from stage 1 $CuCl_2$-GIC. It is obvious that the expected graphite and metallic copper existed in the samples. The signal located at about 28° in 2-theta value can be attributed to the (200) diffraction peak of KCl, which would probably be encapsulated into the gallery since it still existed after the following washing procedures. The XRD patterns of other samples were similar to this (not shown here), but the relative intensities of the diffraction peaks of the copper were different: sample 1 was the strongest, sample 2 was secondary, and sample 3 was the weakest, which means that the copper content was reduced in turn from sample 1 to sample 3. In other words, the copper content in the samples was dependent on GIC stage-structure. The element content, as analyzed by EDS in the Table, was the average value of 10 or more data from different measurement areas. The results show that the order of copper content descended in turn from sample 1 through sample 2 to sample 3, which is in good agreement with the XRD results. The standard deviation of the contents of different measurement areas (Table) was relatively small, which means that the chemical compositions of the samples were uniform.

Electron microscopy analysis

Figure 2 presents the morphology of sample 1 reduced from stage 1 GIC. As the image shows, it was a thin flake with a cured edge, about 1 μm in diameter with a thickness of less than 20 nm, which is extremely thin. When the stage number of the GIC precursors increased, both the thickness and the diameter of the sample flake increased. The thickness of sample 1 was about 20 nm, sample 2 was about 10 nm, and sample 3 was at the micron level. The size in diameter of the products varied from around 1 μm for sample 1 to several microns for sample 2 and larger than 10 μm for sample 3.

Since the copper still remained after the treatment of the acidified $FeCl_3$ solution, it was confirmed that the copper species existed in the sample flake. Figure 3a shows a bright field TEM image of sample 1, in which the nanoparticles are abundant and uniformly distributed rather than gathered on the edge of the flake, very different from the products reduced from $TaCl_5$- and $PdCl_2$-GIC by hydrogen gas[11,12]. The reason may be that the reaction temperature was very low in our experiment and the decomposition of the GIC precursor was avoided. The copper species are round in shape in Figure 3a, and some of them are rectangle. Their sizes, as observed in TEM images, are listed in the Table; the statistical data show that the average size of the nanoparticles was dependent on the stage number of the precursor, with sample 1 being smallest while sample 3 was largest. It can be seen from Figure 3 that most of the nanoparticles were highly transparent, and the underlying particle can be distinguished clearly. This means that the nanoparticles were encapsulated in different graphene and their thickness was very small. As mentioned above, the thickness of the graphene flakes

in sample 1 was less than 20 nm; if the 3 layers of copper species were embedded in it, the thickness of each copper sheet would be just a few nanometers, and the average particle size of these copper species would be 22.5 nm (Table). Thus, the shape of the nanoparticles was a nanoplate, which can be seen as 2-dimensional or quasi-2-dimensional.

Figure 3b is a typical HRTEM image of sample 1. The lattice spacing of 0.2178 nm can be attributed to the graphite (200) plane, and another one with a value of 0.1824 nm was very close to that of the copper (100) plane. The inset figure in Figure 3b (Figure 3c) is a selected area electron diffraction (SAED) pattern of the nanoplate; the image shows 2 diffraction patterns. The pattern with tetragonal-symmetry can be attributed to the diffraction of the Cu [001] crystal zone; the other, with hexagonal-symmetry, to the diffraction of the graphite [001] crystal zone. The near overlapping of the diffraction patterns indicates that the copper was coherently latticed with the graphene.

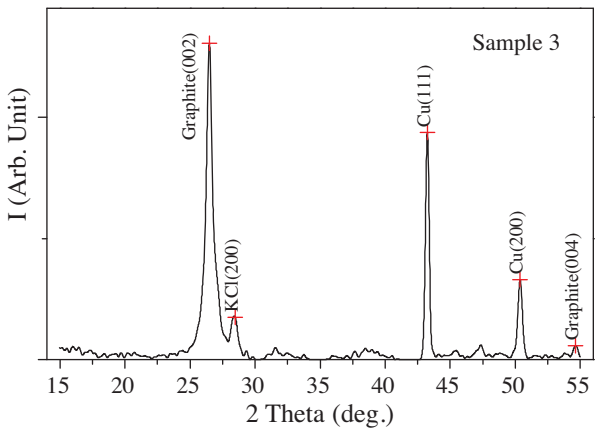

Figure 1. XRD pattern of KBH_4-reduced product from stage 3 GIC (sample 3).

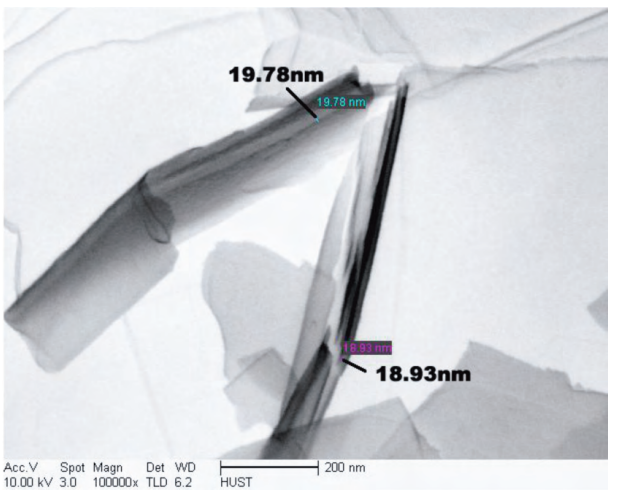

Figure 2. FE-SEM image of reduced product from stage 1 GIC (sample 1).

Interaction between copper nanoplates and graphene

The XPS results showed that there were 2 states for the carbon in all samples. The state of lower binding energy was denoted as A and the higher was denoted as B, for convenience. Figure 4a is the fitting result of C1s for sample 2; the result indicates that the bind energy (BE) of state A was 283.8 eV with a full width at half maximum (FWHM) of 1.5 eV, and the BE of state B was 284.8 with a FWHM of 3.1 eV. The fitting results of all the other samples indicated that the BE and FWHM of state A were unchanged and those of state B were changed with the sample number: in sample 1, BE = 284.7 and FWHM = 2.6 eV, and in sample 3, BE = 285.0 and FWHM = 2.1 eV. State B can be regarded as the intrinsic state of C1s of graphite, while the decrease of the binding energy for state A may be due to the negative charge transfer from the metallic to the hexagonal network.[19] Furthermore, the spectrum of $Cu2p_{3/2}$ indicates that the copper exhibited 2 states as well, and the integrated intensity of the 2 states were almost equal (Figure 4b). For the state of lower energy (state A), the value of BE was 933.4 eV with a FWHM of 2.6 eV, which is in accord with that of bulk copper. For the

state of higher energy (state B), the value of BE ranged from 934.6 to 935.3eV and the FWHM was 3.9-4.4 eV, larger than that of state A. The increase of the binding energy of state B could be attributed to the electron loss of the surface copper atoms. According to the solid-state theory, when 2 types of conductors with different work functions are in contact, the electrons from the conductor with the lower emission work transfers to the other conductor. In the as-prepared samples, the copper with the lower work function was encapsulated by the graphene, so the direct contact between the metal and the graphene network would have made the electron transfer from the surface copper atoms to the graphene carbon atoms. As a result, the loss of negative charge to the copper atoms would enhance the binding energy, and, meanwhile, the binding energy of C1s would decrease. The integration intensity of the state is relative to the concentration of the corresponding atoms in XPS, as mentioned above, and the integration intensity contributed from state A and state B were almost equal, which indicates that the concentrations of the copper atoms in the 2 different states were equal. For a particle with a diameter of 20 nm, as shown with HRTEM, when the concentration of the surface atoms is equal to that of the bulk atoms, the thickness is at most 2.4 nm, which is in good agreement with the analysis results above.

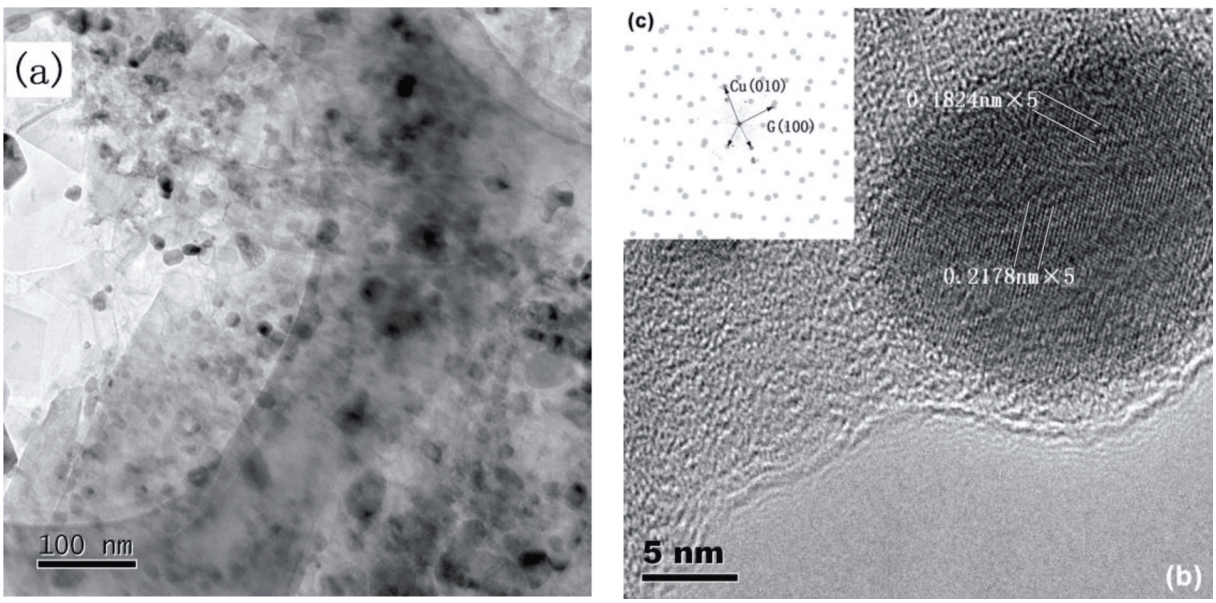

Figure 3. TEM (a) and HRTEM image (b) of reduced product from stage 1 GIC (sample 1); inset (c) is the SAED pattern.

Figure 5 is the Raman spectrum of sample 3; the others were similar to this and are not shown here. The spectra of all samples showed a strong graphitic G band, which split into 2 subbands. The lower frequency subband (E^l_{2g}) was at approximately 1576-1580 cm^{-1} with a FWHM of 16-38 cm^{-1}. The higher frequency subband (E^h_{2g}) was at approximately 1603-1612 cm^{-1} with a FWHM of 16-19cm^{-1}, with an integrated intensity only 0.2-0.4 times that ofE^l_{2g}. The split of the G band indicates that there were 2 states of the hexagonal carbon network; the mode E^h_{2g} would be attributed to the interaction between the metal and graphene, which is in good agreement with the XPS results. Except for the G band and D band at approximately 1327-1334 cm^{-1}, the signals at about 1956 and 852 cm^{-1} would be respectively attributed to the iTOLA mode and the

oTO mode, features of the nonplanar graphene.[20] Two mechanisms would account for this phenomenon. First, it was caused by the laser irradiation. Second, it was caused by the action of the copper nanoplates.

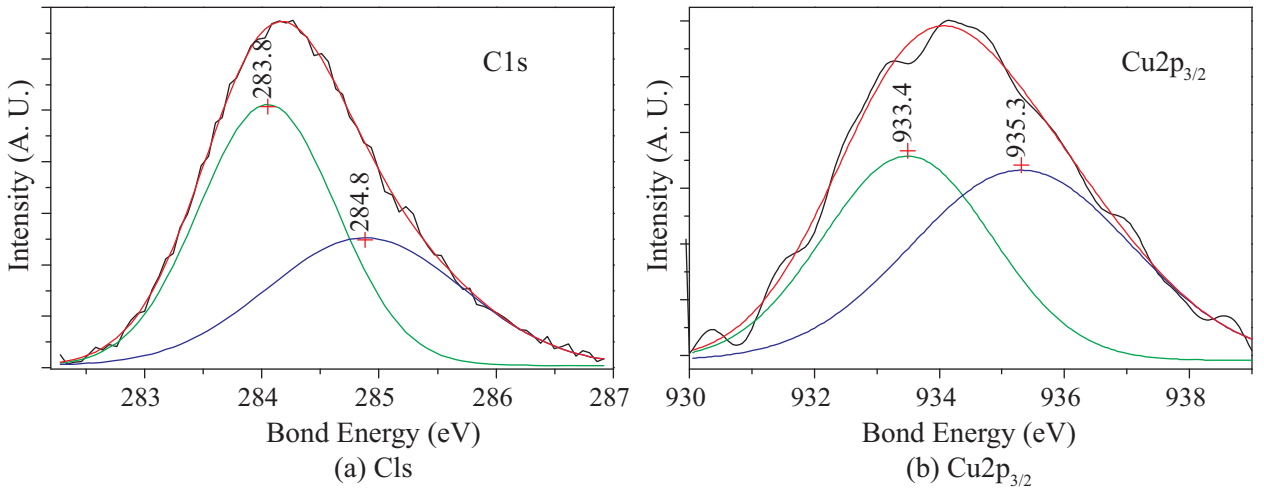

Figure 4. XPS patterns and fitted results of the as-reduced product from stage 2 GIC (sample 2).

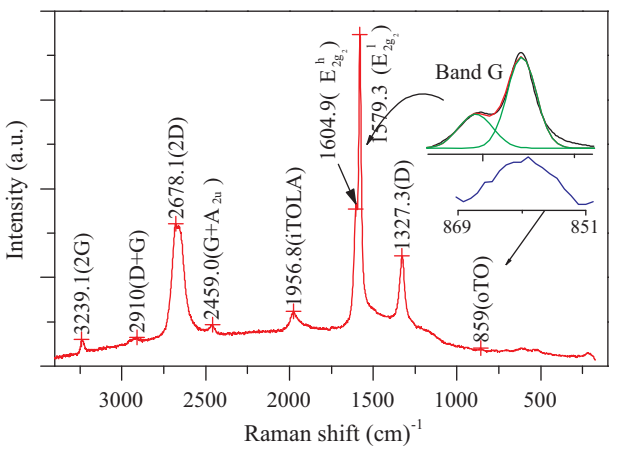

Figure 5. Raman spectrum of the as-reduced product from stage 3 GIC (sample 3).

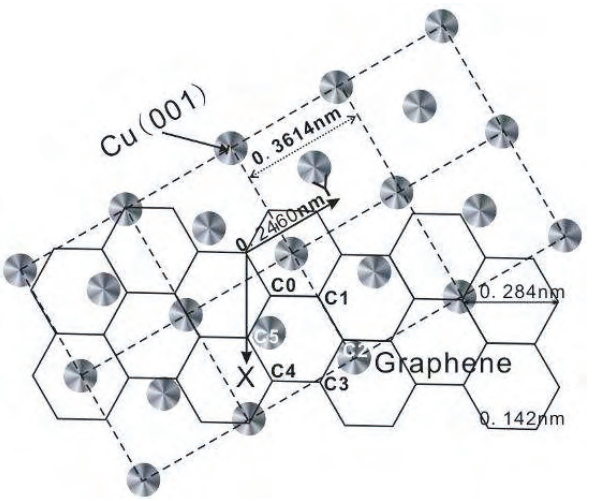

Figure 6. Scheme for structure of graphene and Cu (001) plane.

Controlled growth of copper nanoplate in the graphene gallery

Figure 6 shows the scheme of graphene and the Cu (001) plane; an arbitrary carbon atom was selected as the original point C_0 in the hexagonal carbon net of graphite, and the other 5 atoms in the hexagon were designated as C_1 through C_5 in a clockwise order. The distance from C_5 to C_2 was 0.284 nm, denoted as d_{52}, and from C_0 to C_1 was 0.142 nm, denoted as d_{01}. Meanwhile, in the Cu (001) plane, the distance between copper atoms was 0.3614 nm, denoted as $d_{Cu(100)}$. In this coordinate system, if the Cu (001) plane was rotated with an angle

of 30 ° counterclockwise around the Z-axis, then $2d_{Cu(100)} = 0.723$ nm, $2d_{52} + d_{01} = 5 \times \quad d_{01} = 0.710$ nm, the absolute difference = 0.013 nm, and the relative error = 1.8%. That is, the 2 lattices were matched well, the result of which would be a decrease in the systemic energy. Under this condition, a superlattice with 2×2 $R(30°)$ for copper crystal would be formed in the graphitic gallery. In the electron microscopy analysis, the Cu [001] crystal zone was always in contact with the graphite (100) crystal zone, and the electron diffraction pattern of Cu (200) and graphite (100) was duplicated or with a small angle error, providing evidence for the lattice match. When the copper grew between the graphitic galleries, the crystal orientation was controlled by the hexagonal carbon network, and the thickness of copper species was limited by the finite space in the graphene gallery. Thus, the copper species encapsulated in the graphene gallery could only grow as a 2-dimensional and orientational thin crystal. According to the growth mode, it could be expected that various species of growth-controlled 2-dimensional metal nanoplate could be obtained by reduction of the corresponding metal chloride GIC precursor.

Conclusion

Graphene-encapsulated copper nanoparticles were prepared by reduction of $CuCl_2$- graphite intercalation compounds; the copper species were 2-dimensional or quasi-2- dimensional nanoplates. The growth of copper nanoplate in the gallery was controlled by the graphene. Charge transfer and electron exchange occurred between the metal copper and the graphitic hexagonal network.

Acknowledgements

This work was supported by the National Natural Science Foundation of China (50774071/E0402) and the Science Research Project of the Hubei Provincial Department of Education (D20091505).

References

1. Walter, J.; Heiermann, J.; Dyker, G.; Hara, S.; Shioyama, H. *J. Catal.* **2000**, *189*, 449-455.
2. Shioyama, H. *Carbon* **2003**, *41*, 2882-2884.
3. Sirokman, G.; Mastalir, A.; Molnar, A.; Bartok, M. *Carbon* **1990**, *28*, 35-42.
4. Jung, H. J.; Vannice, M. A.; Mulay, L. N.; Stanfield, M. R.; Delgass, W. N. *J. Catal.* **1982**, *76*, 208-224.
5. Hirai, N.; Takashima, M.; Tanaka, T.; Hara, S. *Sci. Technol. Adv. Mater.* **2004**, *5*, 181-185.
6. Suzuki, I. S.; Suzuki, M.; Walter, J. *Sol. State Commun.* **2001**, *118*, 523-527.
7. Suzuki, M.; Suzuki, I. S.; Wada, N.; Whittingham, M. S. *Phys. Rev. B* **2001**, *64*, 104418-1-8.
8. Bin, X. B.; Chen, J. Z.; Cao, H.; Liu, H. B.; Tu, W. M. *Tribology* **2008**, *28*, 23-27.
9. Shioyama, H.; Min, X. *Carbon* **2004**, *42*, 2127-2130.
10. Ohira, M.; Messaoudi, A.; Inagaki, M.; Beguin, F. *Carbon* **1991**, *29*, 1233-1238.
11. Walter, J. *Adv. Mater.* **2000**, *12*, 31-33.

12. Walter, J. *Synth. Metal.* **1997**, *89*, 39-45.
13. Shioyama, H.; Sakakihara, H.; Enomoto, H.; Iwashita, N.; Tatsumi, K.; Sawada, Y. *J. Mater. Sci. Lett.* **1996**, *15*, 453-454.
14. Bin, X. B.; Tu, W. M.; Zeng, X. B. *J. Wuhan Univ. Technol. (Mater. Ed.)* **1998**, *13*, 39-42.
15. Cao, H.; Wang, X. H.; Bin, X. B.; Chen, L. Q.; Wang, J. H. *Acta Mineral. Sinica* **2005**, *25*, 75-80.
16. Vol'pin, M. E.; Novikov, Y. N.; Lapkina, N. D.; Kasatochkin, V. I.; Struchkov, M. E. *J. Am. Chem. Soc.* **1975**, *97*, 3366-3373.
17. Mizutani, Y.; Abe, T.; Ikeda, K.; Ihara, E.; Asano, M.; Harada, T. *Carbon* **1997**, *35*, 61-65.
18. Bin, X. B.; Chen, J. Z.; Cao, H.; Ma, E. B.; Wang, X. H.; Yuan, J. Z. *Acta Geologica Sinica* **2008**, *82*, 1056-1060.
19. Crist, B. V. *Handbook of Monochromatic XPS Spectra*, Wiley-VCH, New York, 2000.
20. Tan, P. H.; Dimovski, S.; Gogotsi, Y. *Phil. Trans. Roy. Soc. Lond. A* **2004**, *362*, 1-22.